Workspace optimization of parallel robot by using multi-objective genetic algorithm[①]

WANG Jinhong (王进洪)[*], LEI Jingtao[②][*][**]

([*] School of Mechatronic Engineering and Automation, Shanghai University, Shanghai 200444, P. R. China)
([**] Shanghai Key Laboratory of Intelligent Manufacturing and Robotics, Shanghai 200444, P. R. China)

Abstract

For the narrow workspace problem of the universal-prismatic-universal (UPU) parallel robot with fixed orientation, a kind of multi-objective genetic algorithm is studied to optimize the robot's workspace. The concept of the effective workspace and its solution method are given. The effective workspace height (EWH) and global condition number index (GCI) of Jacobi matrix are selected as the optimized objective functions. Setting the robot in two different orientations, the geometric parameters are optimized by the multi-objective genetic algorithm named non-dominated sorting genetic algorithm II (NSGA-II), and a set of structural parameters is obtained. The optimization results are verified by four indicators with the robot's moving platform at different orientations. The results show that, after optimization, the fixed-orientation workspace volume, the effective workspace height and the effective workspace volume increase by 32.4%, 17.8% and 72.9% on average, respectively. GCI decreases by 6.8% on average.

Key words: parallel robot, multi-objective genetic algorithm, workspace optimization

0   Introduction

Compared with traditional serial robots, parallel robots have the advantages of good rigidity, high load capacity and high accuracy, which are widely used in motion simulators, machining machines, manufacturing lines, space docking, and medical applications[1].

Generally, the workspace of parallel robots is limited by the branch chains. To ensure the flexibility and operability of the end-effector, it is important to make the workspace as large as possible to meet the operation requirements. The singularity will affect the performance of parallel mechanism seriously[2], so it is necessary to optimize the robot parameters to get a large and singularity-avoided workspace.

Many scholars have studied workspace optimization of parallel robots. Rios et al.[3] proposed a two-stage optimization method based on a bionic algorithm for designing a Stewart platform. Gao et al.[4] used genetic algorithms and artificial neural networks for dimensional optimization of spatial six-degree-of-freedom parallel robots. Refs[5-8] have used algorithms such as particle swarm algorithms and genetic algorithms for the optimal design of several types of parallel robots

using the workspace, stiffness, load-bearing capacity and dynamic performance parameters as objective functions. Li et al.[9] used a multi-objective particle swarm algorithm to find the optimal singularity-free path. Chi et al.[10] optimized the design variables of a parallel manipulator in terms of both workspace and stiffness. Tu et al.[11] used genetic algorithm to optimize a bumper based on Stewart platform for an inertial navigation system to improve the recovery accuracy. Nabavi et al.[12] used dexterity, kinetic energy and improved workspace index as objective functions for optimization to obtain better workspace and mechanical properties for a general-purpose 6-prismatic-universal-spherical (PUS) parallel robot by using a multi-objective genetic algorithm. Liu et al.[13] analyzed the parametric performance mapping of high-speed parallel robots and optimized the performance parameters of the driving system based on the proposed mapping. Mazare and Taghizadeh[14] used genetic algorithm and harmony search algorithm to optimize the design of Delta parallel robot to obtain larger workspace size and good dynamic performance. Erylmaz and Omurlu[15] used a sequential quadratic programming approach to parametrically optimize the parameters of the 3-universal-prismatic-universal (UPU) platform in order to maximize the

reachable workspace and avoid singularity patterns as much as possible, and finally obtained the optimal motion parameters. Fan et al.[16] proposed a safe workspace verification algorithm and analyzed the singularities of Stewart mechanism in 16 typical extreme poses to provide a reference for optimal design.

In this paper, the workspace of the 6-UPU parallel robot with the fixed orientation is studied. Firstly, the effective workspace is defined. Secondly, the boundary search algorithm and subspace extraction method are adopted to calculate the effective workspace. Thirdly, the effective workspace height (EWH) and global condition number index (GCI) are selected as the optimization objective functions, and the geometric parameters of the robot are optimized by non-dominated sorting genetic algorithm II (NSGA-II). Finally, the optimized results are verified by four indicators of the robot.

1 Inverse kinematic modeling

1.1 6-UPU parallel robot

The 6-UPU robot configuration consists of a fixed platform, a moving platform, six telescopic branch chains and twelve hinges, as shown in Fig.1(a). The single branch chain of the robot is shown in Fig.1(b).

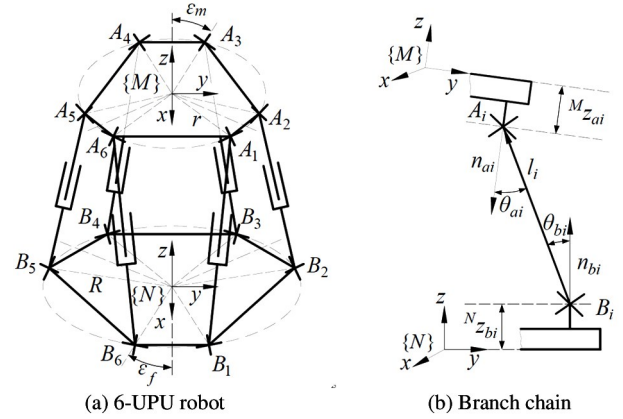The fixed platform coordinate system $\{N\}$ and moving platform coordinate system $\{M\}$ are located at

(a) 6-UPU robot   (b) Branch chain

Fig. 1   Robot configuration

the center of the fixed platform and moving platform, respectively. The hinge points of fixed and moving platform are defined as B_i and A_i in counterclockwise direction, respectively. The position vector of each hinge point of the fixed and moving platform are defined as $\boldsymbol{b}_i$ and $\boldsymbol{a}_i$. The position vector of the i-th branch chain is defined as $\boldsymbol{l}_i(i=1,2,\cdots,6)$.

The position and orientation of the moving platform can be expressed by a vector:

$$\boldsymbol{X} = \begin{bmatrix} p_x & p_y & p_z & \alpha & \beta & \gamma \end{bmatrix} \tag{1}$$

The symbols of the geometric parameters are shown in Table 1.

<p align="center">Table 1   Geometric parameters</p>

Geometric parameters	Symbol
Fixed platform radius	R
Moving platform radius	r
Fixed platform hinge point distribution angle	ε_f
Moving platform hinge point distribution angle	ε_m
Branch chain lengths	l_i
Coordinate value of the lower hinge center along z-axis of $\{N\}$	$^N z_{bi}$
Coordinate value of the upper hinge center along z-axis of $\{M\}$	$^M z_{ai}$
Angle of hinge	θ_{ai} or θ_{bi}

1.2 Inverse kinematics

1.2.1 Inverse solution

The inverse solution of parallel robot is solved by the vector equation method. The length of each branch chain is calculated according to the position and orientation of the moving platform.

The vector diagram of i-th branch chain is shown in Fig.2. The vector equation of i-th branch chain is

$$\begin{aligned} \boldsymbol{l}_i &= {}^N\boldsymbol{p}_{Mo} + {}^N\boldsymbol{a}_i - {}^N\boldsymbol{b}_i \\ &= {}^N\boldsymbol{p}_{Mo} + {}^N_M\boldsymbol{R} \cdot {}^M\boldsymbol{a}_i - {}^N\boldsymbol{b}_i \quad (i=1,2,\cdots,6) \end{aligned} \tag{2}$$

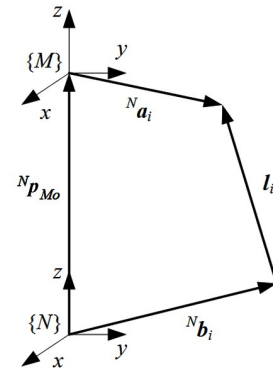**Fig. 2**   Closed-loop vector diagram of i-th branch chain

1.2.2 Velocity analysis

Derivating both sides of Eq. (2) yields:

$$v_i = v_{Mo} + \omega_M \times {}_M^N R \cdot {}^M a_i \quad (i = 1,2,\cdots,6) \tag{3}$$

where v_i is the velocity vector of the electric cylinder of the branch chain; v_{Mo} and ω_M are the linear velocity vector and angular velocity vector of the moving platform, respectively.

Multiplying both sides of Eq. (3) by the directional unit vector of the branch chain, the velocity of branch chain is derived as

$$v_i = \begin{bmatrix} s_i^T & ({}_M^N R \cdot {}^M a_i \times s_i)^T \end{bmatrix} \begin{bmatrix} v_{Mo} \\ \omega_M \end{bmatrix}$$
$$(i = 1,2,\cdots,6) \tag{4}$$

where s_i is the directional vector of each branch chain.

The velocity inverse solution can be written as

$$v = J \dot{X} \tag{5}$$

where $v = \begin{bmatrix} v_1, & v_2, & v_3, & v_4, & v_5, & v_6 \end{bmatrix}^T$, $\dot{X} = \begin{bmatrix} v_{Mo} & \omega_M \end{bmatrix}^T$.

Then the velocity Jacobi matrix of the robot is derived as

$$J = \begin{bmatrix} s_1^T & ({}^N a_1 \times s_1)^T \\ s_2^T & ({}^N a_2 \times s_2)^T \\ \vdots & \vdots \\ s_6^T & ({}^N a_6 \times s_6)^T \end{bmatrix} \tag{6}$$

2 Effective workspace

2.1 Effective workspace introduction

For the robot fixed-orientation workspace, there is a part of shaded area shown in Fig. 3, in which the robot's motion path is partly discontinuous, so this part is almost unusable. Therefore, the area with continuous paths in the fixed-orientation workspace is defined as the effective workspace.
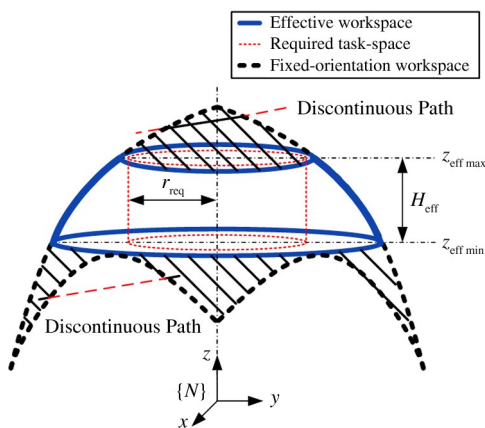

Fig. 3 Diagram of the effective workspace

It is assumed that the required task-space of the robot operation task is a cylinder shown in the area of the thin dotted line in Fig. 3. The radius of the cylinder r_{req} is used to reflect the size of the required task-space.

The area in the real line shown in Fig. 3 is effective workspace, it should be larger than the required task-space so as to meet the operating task requirements.

The effective workspace of the robot is composed of a series of effective subspaces. For each effective subspace, it should satisfy that the vertical distance from any boundary point to z-axis is greater than or equal to the radius of the required task-space:

$$\forall \| p_j \|_2 \geqslant r_{req} \quad j = 0,1,2,\cdots,m \tag{7}$$

where $\| \cdot \|_2$ is the 2-norm of a vector, p_j is the vector of j-th boundary point in subspace, r_{req} is the radius of the required task-space, m is the number of boundary points in a subspace.

EWH can be used to reflect the volume of the area satisfying required task-space. EWH can be obtained as

$$H_{eff} = z_{effmax} - z_{effmin} \tag{8}$$

where, z_{effmax} is the maximum value of effective subspace in z-axis, z_{effmin} is the minimum value of effective subspace in z-axis.

2.2 Effective workspace calculation

The center point of the moving platform is selected as the reference point to study the effective workspace. Firstly, the boundary points of the robot workspace can be obtained by the boundary search algorithm. Secondly, the effective workspace can be calculated by the subspace extraction method.

2.2.1 Boundary search algorithm

(1) All known geometric parameters are input, then the given orientation angle is input, the search range of the robot workspace and the search step are initially determined according to the geometric parameters. The polar coordinate system is used to describe the workspace.

(2) According to the search step described above, the search space is divided into several subspaces z_i.

For a subspace, it can be divided into a number of points by pole angle and pole diameter. Each point can be judged whether it is in the workspace according to the constraints after inverse kinematics. The boundary point can be obtained and saved to the boundary point set.

2.2.2 Subspace extraction method

(1) After obtaining all boundary points in the

plane of z_i subspace, Eq. (7) is used to judge whether the subspace is an effective subspace. If yes, save all boundary points in the plane to the set of effective boundary points before proceeding to the next step; if no, proceed to the next step direct.

(2) Determining whether the subspace plane has reached the highest value of the search range. If yes, then all effective workspace point sets are obtained; if no, then turn to the boundary search algorithm to search the next subspace plane.

(3) The boundary points are saved to the corresponding point sets, then the workspace parameter, EWH, can be further obtained by calculating the point sets.

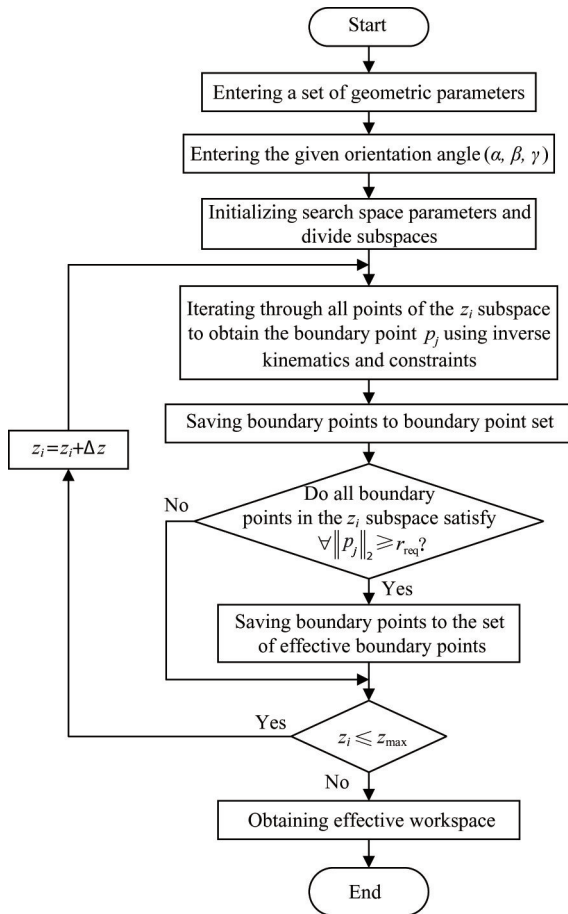The calculating flowchart of the effective workspace is shown in Fig. 4.

Fig. 4 Calculating flowchart of the effective workspace

When the moving platform of the robot is at the initial orientation (0°, 0°, 0°), and a set of parameters of robot is set as $R = 150$ mm, $r = 90$ mm, $\varepsilon_f = 15°$, $\varepsilon_m = 15°$, $l_i = 350 - 500$ mm, ${}^N z_{bi} = 60$ mm, ${}^M z_{ai} = 40$ mm, $\theta_{ai} = 0 - 40°$, $\theta_{bi} = 0 - 40°$, the required task-space radius is assumed as $r_{\rm req} = 50$ mm,

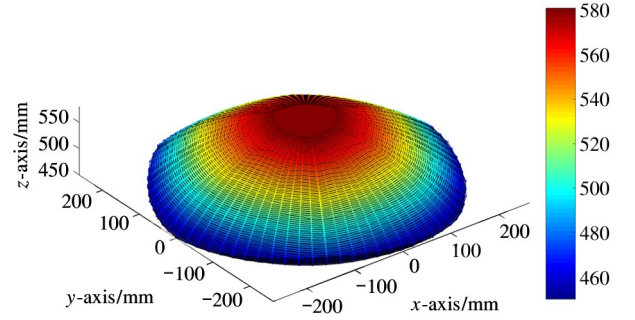the calculation result of the effective workspace is shown in Fig. 5.

Fig. 5 Effective workspace of the robot with the moving platform at the initial orientation

3   Workspace optimization

The multi-objective genetic algorithm NSGA-II with the properties of a fast non-dominated sorting procedure and an elitist strategy[17] is adopted to optimize the robot's workspace.

3.1   Objective functions

Two indexes are selected as the objective functions. As EWH can reflect the volume of the area satisfying required task-space, it is selected as an objective function. GCI indicates the dexterity of the robot, which is an average value of the local condition number index (LCI) of Jacobi matrix. The smaller GCI is, the better the robot's dexterity is.

To avoid the robot from singularity, GCI is selected as the other objective function.

$$\min f = (f_1, f_2)$$
$$f_1 = -H_{\rm eff}$$
$$f_2 = {\rm Cond}_{\rm Global}(\boldsymbol{J}) = \frac{1}{n}\sum_{i=1}^{n}{\rm Cond}_{\rm local}(\boldsymbol{J})_i \tag{9}$$

3.2   Design variables and constraints

Eight geometric parameters of the robot related to the objective functions are summarized in Table 1. For simplicity, the design variables are reduced to four, i. e. the moving platform radius R, the fixed platform radius r, the moving platform hinge distribution angle ε_m, and the fixed platform hinge distribution angle ε_f.

The constraints of optimization are

$$\text{s. t.} \begin{cases} 80\ {\rm mm} \leqslant r \leqslant 120\ {\rm mm} \\ 100\ {\rm mm} \leqslant R \leqslant 200\ {\rm mm} \\ 10° \leqslant \varepsilon_m \leqslant 30° \\ 10° \leqslant \varepsilon_f \leqslant 30° \\ r \leqslant R \end{cases} \tag{10}$$

3.3 Optimization results

After optimization, two objective function values are shown in Fig. 6.

It can be seen from Fig. 6 that while the absolute value of EWH increases, GCI increases, so it is difficult to obtain larger workspace and better dexterity at the same time. Ten sets of the individuals with two kind of different orientation angles from Fig. 6 are shown in Table 2 and Table 3, respectively.
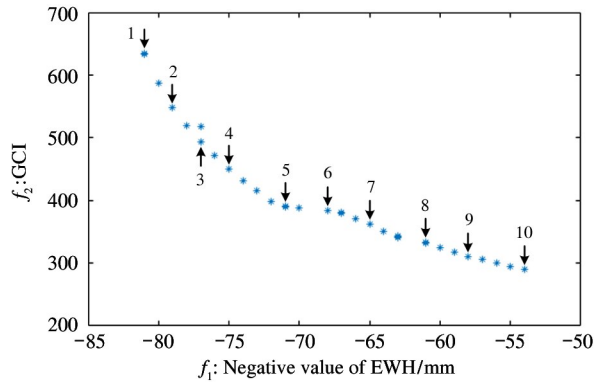
(a) Orientation angle is (15°, 15°, 15°)
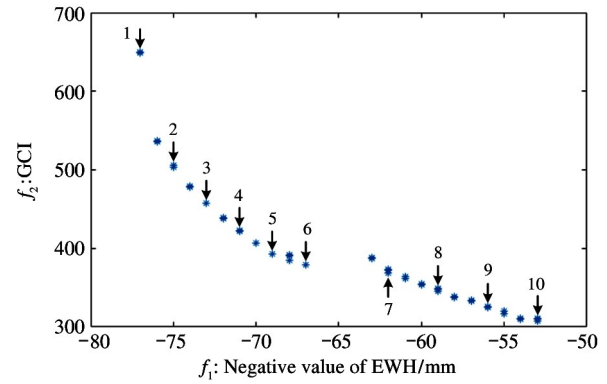
(b) Orientation angle is (−15°, −15°, −15°)

Fig. 6   Two objective function values after optimization

Table 2   Ten sets of individuals with the orientation angle (15°, 15°, 15°)

Individual No.	r/mm	R/mm	ε_m/°	ε_f/°	−EWH/mm	GCI
1	80.0000	101.1724	12.0923	14.0539	−81	633
2	80.0000	113.5998	11.9490	13.7714	−79	548
3	80.0000	123.6714	12.0128	13.4148	−77	493
4	80.0000	133.2588	11.8964	13.5028	−75	450
5	80.0299	146.3463	11.5028	12.6483	−71	389
6	82.5485	150.2424	13.2710	10.0781	−68	384
7	83.1565	158.7335	13.3758	10.0000	−65	362
8	83.0915	174.0191	13.8098	11.2004	−61	332
9	83.4855	181.5173	13.7999	10.4943	−58	310
10	83.6011	191.1415	13.8149	10.5342	−54	290

Table 3   Ten sets of individuals with the orientation angle (−15°, −15°, −15°)

Individual No.	r/mm	R/mm	ε_m/°	ε_f/°	−EWH/mm	GCI
1	80.0000	108.0237	19.8545	10.0000	−77	649
2	80.0987	119.9570	11.5570	13.3245	−75	504
3	80.0178	121.3746	10.6967	10.4401	−73	458
4	80.0075	130.4480	10.7268	10.6922	−71	422
5	80.0000	136.2511	10.4789	10.0000	−69	392
6	80.0861	142.7174	10.6786	10.9460	−67	379
7	80.5778	180.0397	10.6342	21.2102	−62	368
8	81.3832	183.9055	10.2145	20.1675	−59	346
9	81.4823	193.1040	10.1881	20.1682	−56	324
10	80.5367	199.9820	10.3817	20.2106	−53	308

From Table 2 and Table 3, it can be seen that when two objective functions are the middle values, the robot not only has larger workspace, but also has better dexterity. Therefore, No. 5 individual in Table 2 and No. 6 individual in Table 3 are selected as the optimal individuals.

The final optimization result can be determined by averaging the optimal parameters obtained with two orientation angles. The optimized parameters of the robot are shown in Table 4.

Table 4   Optimized parameters

Symbol	r /mm	R /mm	ε_m /°	ε_f /°
Value	81.09	144.64	14.575	13.13

4   Validation

Changing the orientation angles of the moving platform around the x-axis or z-axis from -30 ° to $+30$ ° by 1 ° step, the optimization results are verified by calculating four indicators. As the robot rotation around the x-axis is similar to that around the y-axis, the orientation taking around the y-axis is omitted.

Selecting four indicators for optimization verification, which are fixed-orientation workspace volume (FWV), EWH, effective workspace volume (EWV) and GCI, EWH and GCI can be calculated by Eq. (8)
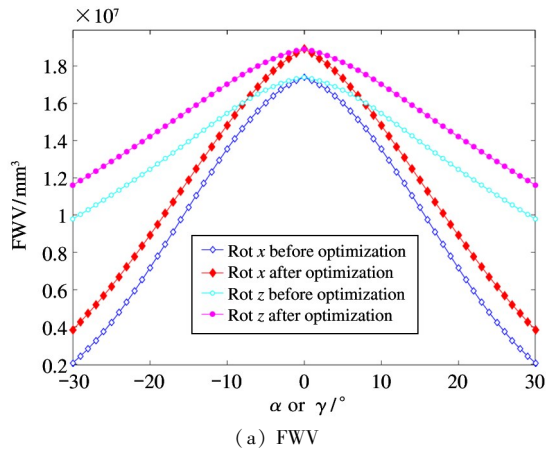
and Eq. (9), while FWV and EWV are calculated by Eq. (11) and Eq. (12)[18], respectively.

$$V_{FW} = \sum_{i=1}^{i_{max}} \sum_{j=1}^{j_{FWmax}} \left(\frac{1}{2} \Delta\theta \rho_i^2 \Delta z \right) \tag{11}$$

where $i_{max} = 2\pi/\Delta\theta$, $j_{FW\,max} = (z_{max} - z_{min})/\Delta z$.

$$V_{EW} = \sum_{i=1}^{i_{max}} \sum_{j=1}^{j_{EWmax}} \left(\frac{1}{2} \Delta\theta \rho_i^2 \Delta z \right) \tag{12}$$

where $j_{EW\,max} = (z_{effmax} - z_{effmin})/\Delta z$.

The parameters of robot before optimization are set as $r = 93.3$ mm, $R = 174.29$ mm, $\varepsilon_m = 22.03$ °, $\varepsilon_f = 10.53$ °, and the optimized parameters are shown in Table 4. The calculation results of four indicators are compared as shown in Fig. 7. The abscissa represents the rotation angle of moving platform around x-axis or z-axis.

(a) FWV
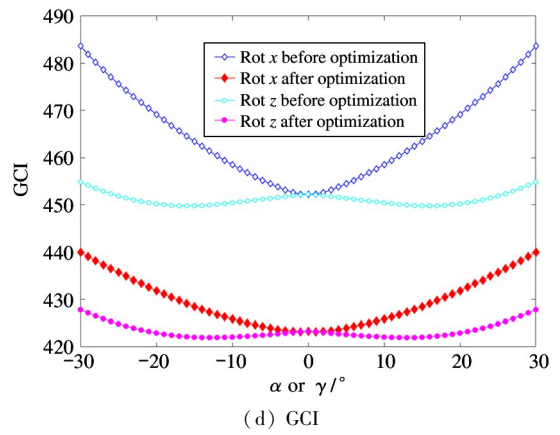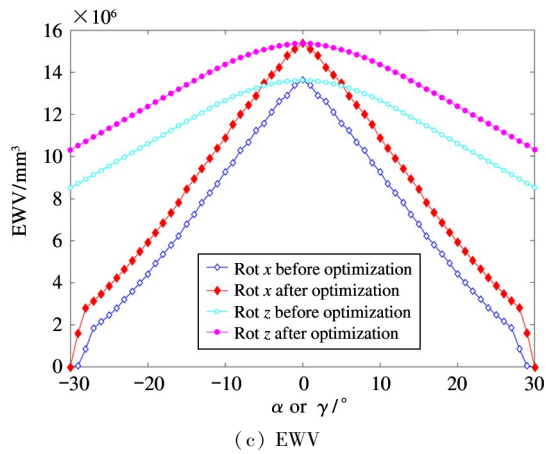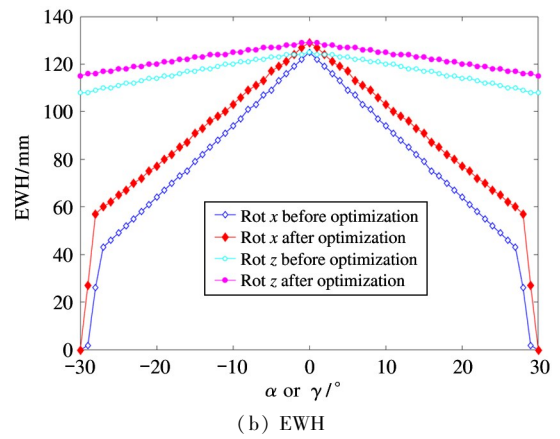

(b) EWH

(c) EWV

(d) GCI

Fig. 7   Comparison of four indicators (before and after optimization)

Fig. 7 shows that FWV, EWH and EWV increased and GCI decreased for all orientation angles used for validation. Specifically, FWV, EWH and EWV increased by 32.4%, 17.8%, and 72.9% on average, respectively, and GCI decreased by 6.8% on average. It is demonstrated that the optimization pa-

rameters enable the robot to have reasonable workspace and better dexterity.

5   Conclusions

(1) The inverse kinematic of the 6-UPU parallel

robot is derived, and the effective workspace solving method is presented, which is the boundary search method and subspace extraction method.

（2）The NSGA-II is adopted to optimize the robot parameters with two objective functions, which are EWH and GCI. A set of optimal parameters of parallel robot can be obtained.

（3）Four indicators of the robot before and after optimization with different orientation angles are compared. The results show that FWV, EWH and EWV increased, GCI decreased. The results show that the workspace optimization method is reasonable.

References

[1] HUANG X G, HE G P, TAN X L, et al. An introduction to parallel robot mechanism [J]. *Journal of North China University of Technology*, 2009, 21(3): 25-31

[2] LI B K, LIU K, HAN Y G, et al. Position singularity-free workspace analysis of the Gough-Stewart parallel mechanism [J]. *Journal of Machine Design*, 2017, 34(10): 61-67

[3] RIOS A, HERNANANDEZ E E, VALDEZ S I. A two-stage mono- and multi-objective method for the optimization of general UPS parallel manipulators [J]. *Mathematics*, 2021, 9(5): 543-562

[4] GAO Z, ZHANG D, GE Y J. Design optimization of a spatial six degree-of-freedom parallel manipulator based on artificial intelligence approaches [J]. *Robotics and Computer Integrated Manufacturing*, 2010, 26(2): 180-189

[5] WU C Y, QIAN X W, YU W, et al. Workspace analysis and optimization of linear driven parallel robot [J]. *Transactions of the Chinese Society for Agricultural Machinery*, 2018, 49(1): 381-389

[6] YANG H, FANG H R, LI D, et al. Kinematics analysis and multi-objective optimization of a novel parallel perfusion robot [J]. *Journal of Beijing University of Aeronautics and Astronautics*, 2018, 44(3): 568-575

[7] ZHANG F, ZHANG B, ZHOU F, et al. Configuration selection and parameter optimization of redundantly actuated cable-driven parallel robots [J]. *Journal of Mechanical Engineering*, 2020, 56(1): 1-8

[8] SUN X Y, ZHENG B, BAO J, et al. Parameter optimization design of high-speed 6-PSS parallel robot [J]. *Transactions of the Chinese Society for Agricultural Machinery*, 2015, 46(5): 372-378

[9] LI S Q, CHEN D, WANG J F. An optimal singularity-free motion planning method for a 6-DOF parallel manipulator [J]. *Industrial Robot*, 2021, 48(2): 290-299

[10] CHI Z Z, ZHANG D, XIA L, et al. Multi-objective optimization of stiffness and workspace for a parallel kinematic machine [J]. *International Journal of Mechanics and Materials in Design*, 2013, 9(3): 281-293

[11] TU Y Q, YANG G L, CAI Q Z, et al. Optimal design of SINS's Stewart platform bumper for restoration accuracy based on genetic algorithm [J]. *Mechanism and Machine Theory*, 2018, 124: 42-54

[12] NABAVI S N, SHARIATEE M, ENFERADI J, et al. Parametric design and multi-objective optimization of a general 6-PUS parallel manipulator [J]. *Mechanism and Machine Theory*, 2020, 152: 1-15

[13] LIU X J, HAN G, XIE F G, et al. A novel parameter optimization method for the driving system of high-speed parallel robots [J]. *Journal of Mechanisms and Robotics*, 2018, 10(4): 1-11

[14] MAZARE M, TAGHIZADEH M. Geometric optimization of a Delta type parallel robot using harmony search algorithm [J]. *Robotica*, 2019, 37(9): 1494-1512

[15] ERYLMAZ C, OMURLU V E. SQP optimization of 6-DOF 3x3 UPU parallel robotic system for singularity free and maximized reachable workspace [J]. *Journal of Robotics*, 2019, 2019(1): 1-14

[16] FAN X W, YANG L L, CHENG Y, et al. Research on optimal configuration design method of Stewart platform [J]. *Journal of System Simulation*, 2020, 32(10): 1981-1988

[17] DEB K, PRATAP A, AGARWAL S, et al. A fast and elitist multiobjective genetic algorithm: NSGA-II [J]. *IEEE Transactions on Evolutionary Computation*, 2002, 6(2): 182-197

[18] LEI J T, CAO Y L, WANG F. Workspace analysis of a 4UPS-UPU parallel mechanism based on the boundary search method [J]. *Machine Design and Research*, 2013, 29(1): 5-9

WANG Jinhong, born in 1998. He received his B. S. degree from Shandong University of Science and Technology in 2020. Now he is a postgraduate student in School of Mechatronic and Engineering Automation, Shanghai University. His research interest is medical robot.